

The observed properties of Fast Radio Bursts

Vikram Ravi^{1*}

¹*Cahill Center for Astronomy and Astrophysics, MC 249-17, California Institute of Technology, Pasadena, CA 91125, USA.*

ABSTRACT

I present an empirical study of the properties of fast radio bursts (FRBs): Gigahertz-frequency, dispersed pulses of extragalactic origin. I focus my investigation on the sample of seventeen FRBs detected at the Parkes radio telescope with largely self-consistent instrumentation. Of this sample, six are temporally unresolved, eight exhibit evidence for scattering in inhomogeneous plasma, and five display potentially intrinsic temporal structure. The characteristic scattering timescales at a frequency of 1 GHz range between 0.005 ms and 32 ms; moderate evidence exists for a relation between FRB scattering timescales and dispersion measures. Additionally, I present constraints on the fluences of Parkes FRBs, accounting for their uncertain sky-positions, and use the multiple-beam detection of FRB 010724 (the Lorimer burst) to measure its fluence to be 800 ± 400 Jy ms. FRBs, including the repeating FRB 121102, appear to manifest with a plethora of characteristics, and it is uncertain at present whether they share a common class of progenitor object, or arise from a selection of independent progenitors.

Key words: catalogues — methods: data analysis — pulsars: general — radio continuum: general — scattering

1 INTRODUCTION

A fast radio burst (FRB) may be broadly defined (cf. Petroff et al. 2015; Keane & Petroff 2015) as a demonstrably astrophysical, dispersed radio pulse, with a dispersion measure (DM) that significantly exceeds any estimate (e.g., Cordes & Lazio 2002) of the Milky Way free-electron column density along its sightline. Implicit in this definition is the condition that FRBs adhere to the cold, sparse plasma dispersion law (e.g., Katz 2016). The identification of the host galaxy of the repeating FRB 121102 (Chatterjee et al. 2017) has confirmed the existence of extragalactic sources of pulsed radio emission. Questions regarding the origins of FRBs may therefore be framed in terms of what kinds of sources, at what extragalactic distances, produce FRBs.

Twenty-four FRB detections have now been published.¹

Even among this small sample, the diversity of FRB properties is striking. FRB 121102, the sole detection at the Arecibo Observatory, is also the only known repeater. Additionally, different FRBs display markedly different propagation signatures; for example, the timescales by which FRBs are temporally broadened during propagation by scattering due to plasma-density inhomogeneities vary by four orders of magnitude (Ravi et al. 2016). Third, as I shall show, even among the sample of seventeen FRBs detected at the Parkes telescope, the range of fluences spans three orders of magnitude.

The primary goal of this paper is to homogenise the inference of FRB properties among the Parkes sample (§2). In particular, I focus on self-consistent estimates of FRB fluences, DMs, intrinsic widths, and scattering timescales and frequency-dependencies. Such measurements have been compiled (and performed) by Petroff et al. (2016), and disseminated through the online FRB catalogue. However, the Bayesian parameter estimation and model selection framework that I apply herein reveals some potential inaccuracies in previous results. I do not attempt to model FRBs

* E-mail: vikram@caltech.edu

¹ A catalogue of FRBs is maintained at <http://www.astronomy.swin.edu.au/pulsar/frbcat/> (Petroff et al. 2016).

with irregular temporal profiles (Champion et al. 2016). I estimate the fluences of the Parkes FRBs by analysing the sky-response model (Ravi et al. 2016) of the thirteen-beam multibeam receiver (MBR; Staveley-Smith et al. 1996) used to detect these events. The fluences of FRBs detected in individual beams of the MBR may be bounded by making use of their non-detections in other beams. Further, for the multiple-beam FRB 010724 (Lorimer et al. 2007), I better constrain its fluence by applying the technique developed by Ravi et al. (2016) for the multiple-beam FRB 150807.

Various attempts have been made to infer characteristics of the FRB population by inspecting the distributions of FRB properties. Efforts have focused in particular on FRB fluences, DMs and scattering timescales. Caleb et al. (2016) and Li et al. (2016) have attempted to use quoted fluences or fluence lower-limits to derive the cumulative fluence distribution (the ‘logN-logF’) for FRBs, and thus test for whether the FRB population is consistent with Galactic, nearby extragalactic, or cosmological origins. However, Vedantham et al. (2016) concluded that the FRB logN-logF is best estimated by analysing the numbers of single- and multiple-beam detections at Parkes, and by comparing detection rates at different telescopes (see also Connor et al. 2016). Additionally, Katz (2016), Vedantham et al. (2016) and Cordes et al. (2016) show that the distribution of FRB DMs is difficult to draw conclusive inferences from. However, Katz (2016) and Cordes et al. (2016) find that the combination of DM and scattering measurements may provide an interesting probe of the characteristic host environments of FRBs. Here, I use updated scattering measurements to revisit the analysis of Cordes et al. (§2.4), and find moderate evidence for a relation between FRB DMs and scattering timescales.

Finally, I discuss the possibility of multiple classes of FRB (§4). I focus on the comparison between the Parkes and Arecibo FRB surveys, which have been undertaken with similar instrumentation, at similar frequencies, but with sensitivities and sky-coverages that differ by more than an order of magnitude. It appears possible that Parkes could already have detected up to three repeating FRBs like FRB 121102. Using my analysis of the Parkes FRB sample, I speculate on which FRBs may be expected to repeat. I also consider whether all Parkes FRBs could be emitted by objects like the source of FRB 121102, and find that, if so, the population must present an incredible diversity of properties. I conclude in §5.

2 MODELLING OF FRB DATA

In the sub-sections below, I first describe the FRB data that I model, including the pre-processing steps that I perform (§2.1). I then outline the different models that I attempt to fit to the data, as well as the Monte Carlo Markov Chain (MCMC) exploration of the model likelihoods and the Bayes Information Criterion used to perform model selection (§2.2). The results of the modelling in this section

Table 1. Properties of FRB detection instruments.

	AFB	BPSR
Centre frequency (MHz)	1372.5	1382.0
Filterbank	Analogue	Digital (4-tap polyphase)
Channel bandwidth (MHz)	3.0	0.390625
Number of channels	96	1024
Integration time (μ s)	125	64
Bits per sample	1	2
σ_i (Jy ms)	0.14	0.11

are presented in Table 2, and discussed in detail in §2.3. I outline the implications of my results for a possible relation between DM and scattering strength in §2.4.

2.1 Description of data and pre-processing

Each Parkes FRB was detected in ‘filterbank’ data recorded for each beam of the 13-beam 21 cm Multibeam receiver (the MBR). Filterbank data are total-power measurements (Stokes I) in numerous spectral channels, integrated over sub-millisecond timescales. FRBs 010125 (Burke-Spolaor & Bannister 2014), 010621 (Keane et al. 2012) and 010724 (Lorimer et al. 2007), were detected in data taken with the Parkes Analogue Filterbank (AFB; Manchester et al. 2001), which performed the channelisation and integration steps prior to (one-bit) digitisation. The remaining FRBs were detected with the Berkeley-Parkes-Swinburne Recorder (BPSR) digital-spectrometer system (Keith et al. 2010), with either ‘iBOB’ or ‘ROACH’ digital signal processing cards developed by the Center for Astronomy Signal Processing and Electronics Research (CASPER), with identical firmware implementations.² Details of the AFB and BPSR instruments are given in Table 1.

For all Parkes FRBs besides 131104 (Ravi et al. 2015) and 150807 (Ravi et al. 2016), the raw filterbank data are made available through the FRB Catalogue (Petroff et al. 2016). For FRB 131104, I made use of raw filterbank data that I have direct access to, which I make publicly available with this publication. For FRB 150807, I make use of raw filterbank data made publicly available by Ravi et al. (2016). The DSPSR package (van Straten & Bailes 2011) was used to dedisperse the filterbank data and extract 2-second duration PSRCHIVE-format (Hotan et al. 2004) data files at the native time and frequency resolutions. Dedispersion was done according to the published DMs for each burst, which I term DM_{init} . For the BPSR data, channels 0 to 160 (1519.5–1582 MHz) were excluded in the analysis, because these frequencies were attenuated in the analogue signal chain to

² The open-source CASPER hardware designs and firmware are described online at <https://casper.berkeley.edu>, and reviews of current CASPER developments are detailed by Hickish et al. (2016).

exclude radio-frequency interference (RFI). No further RFI excision was done. Persistent, narrow-band RFI did not significantly affect the analysis both because of the level-setting procedures of the AFB and BPSR instruments, and because I also subtracted a mean off-pulse baseline level from each channel in the 2-second datasets. Additionally, I searched for significantly time-variable or exceedingly strong (comparable to the system temperature) narrow-band RFI by inspecting the total-power variances of each channel in the data, but found none at the 3σ level. I also found no significant bursts of RFI (narrow- or broad-band) coincident with any of the FRBs.

To accelerate further analysis, the dedispersed data were averaged to four channels within the respective AFB and BPSR bands. In each channel, the data were further normalised by the off-pulse standard deviations at a fiducial integration time of 1 ms.

FRB 010724 was detected in four beams of the MBR, and saturated the 1-bit digitiser of the AFB in the primary detection beam (beam 6; Lorimer et al. 2007). I therefore analysed a dataset formed from the sum of the three other detection beams (beams 7, 12 and 13).

2.2 Multi-frequency burst profile modelling

The pulse-modelling technique employed here closely follows that employed by Ravi et al. (2015) for FRB 131104. I used a Bayesian technique to find model parameter values that best fit the data, as well as their confidence intervals. This technique fully accounts for covariances between model parameters, and allows for accurate parameter confidence intervals in the case of non-Gaussian posterior distributions to be presented. I used the *emcee* MCMC software package (Foreman-Mackey et al. 2013) to explore the full likelihood spaces of the multi-frequency models given the data. Following a burn-in stage, the joint posterior density of all parameters was estimated with 48000 samples.

To select between models with varying numbers of free parameters, the Bayes Information Criterion (BIC) was calculated for each analysis. The BIC is given by $-2 \ln \hat{L} + k[\ln n - \ln(2\pi)]$, where \hat{L} is the likelihood estimate for a model with fully specified parameters, k is the number of model parameters, and n is the number of measurements being fit to. In accordance with common practise, I selected the model with the lowest BIC, unless there was a model with fewer free parameters with a BIC within three units of the lowest BIC, in which case the model with the fewer free parameters was selected.

The general statistical model that I adopt for the data is outlined in the Appendix. Four specific models were considered, as described below.

Model 0. This model represents a pulse that is temporally unresolved by the instrument, such that the measured shape at each frequency is set by the mean intra-channel dispersion smearing of a delta-function impulse. The contribution to the measured pulse width from the impulse response

of the instrument, quantified approximately as the inverse of the channel bandwidth (Cordes & McLaughlin 2003), is negligible, and I hence do not include it in the model. Given a channel response function $\hat{g}(\nu)$ (e.g., Equation A6), where ν is the radio frequency, the dispersion-smearing temporal profile of a delta-function impulse is given by writing ν in terms of the corresponding dispersion delay (Equation 2 below). The AFB and BPSR channel responses are both well modelled by Gaussian functions. The model pulse profile in a channel with frequency ν_i is given by

$$S_i(t) = \frac{c_i}{\sqrt{2\pi\sigma_{i,\text{DM}}^2}} \exp\left[-\frac{(t - t_0 - t_{i,\text{DM}})^2}{\sigma_{i,\text{DM}}^2}\right], \quad (1)$$

where t_0 is a reference time at the highest frequency,

$$t_{i,\text{DM}} = (4.15 \text{ ms}) \text{DM}_{\text{err}}[(\nu_i/\text{GHz})^{-\beta} - 1.582^{-\beta}] \quad (2)$$

with $\beta = 2$, and

$$\sigma_{i,\text{DM}} = (1.622 \times 10^{-3} \text{ ms}) \text{DM}(\nu_i/\text{GHz})^{-\beta-1}. \quad (3)$$

Here, DM_{err} is the deviation of the burst DM from that assumed in the initial dedispersion of the filterbank data (DM_{init}), and DM is $\text{DM}_{\text{init}} + \text{DM}_{\text{err}}$. The coefficients c_i are proportional to the burst fluences in each of the four frequency channels (indexed by i), not accounting for the uncertain positions of the FRBs within the Parkes response function on the sky. Representative constants of proportionality, σ_i , assuming beam-boresight positions are given in Table 1 for the AFB and BPSR systems. I assume a frequency-independent system temperature of 28 K, a gain of 1.45 Jy K^{-1} , and digitization-loss factors of 0.798 and 0.936 respectively for the AFB and BPSR (Keane & Petroff 2015).

The model free parameters are therefore the four c_i coefficients, t_0 and DM_{err} . Note that the assumption of $\beta = 2$ implies that I assume cold, sparse plasma dispersion; no significant deviations from $\beta = 2$ have been detected for any FRB, and when relaxing this assumption I also did not find any significant deviations. Although the constraining range on β can be used to constrain the size of the dispersing region (Masui et al. 2015), my work does not improve on existing results, and I hence do not report that part of the analysis.

Model 1. This model is the same as Model 0, with the modification of setting $\sigma_{i,\text{DM}}$ to $(\sigma_{i,\text{DM}}^2 + \zeta^2)^{1/2}$. Here, the new free parameter ζ is an intrinsic burst width. I assume a Gaussian intrinsic profile, in accordance with common practise in modelling the mean pulse profiles of pulsars (e.g., Yan et al. 2011). The quality of the data also do not permit exploration of more complex profiles in most cases.

Model 2. This model extends Model 0 by including the effects of temporal broadening due to scattering, clearly detected in some FRBs with high signal-to-noise ratios, such as FRB 110220 (Thornton et al. 2013) and FRB 131104 (Ravi et al. 2015). I account for scattering by convolving the temporal profile in Equation 1 with a one-sided exponential

function:

$$s_i(t) = \exp\left[\frac{t - t_0}{\tau_{1\text{ GHz}} \nu_{i,1}^{-\alpha}}\right], \quad t > 0 \quad (4)$$

$$= 0, \quad \text{otherwise.} \quad (5)$$

Here, $\nu_{i,1}$ is the frequency of channel i expressed in units of 1 GHz. This form for the pulse-broadening function implicitly assumes that the scattering medium can be well approximated by density inhomogeneities projected onto a single thin screen (Cronyn 1970). However, none of the FRB data have sufficient sensitivity to distinguish between this and other subtly different forms (e.g., Williamson 1972). The new free parameters are the characteristic broadening timescale at 1 GHz, $\tau_{1\text{ GHz}}$, and the index of frequency-dependency, α .

In some cases, this model was preferred over all others according to the BIC, but the value of α was poorly constrained. In these cases, I assumed a value of $\alpha = 4$ to estimate $\tau_{1\text{ GHz}}$, corresponding to the expectation for a normal distribution of plasma-density inhomogeneities. In one other case (FRB 140514), there was insufficient sensitivity to distinguish between this model and Model 1. I assumed Model 1 in this case.

Model 3. This model combines Models 0–2, including the effects of both scattering and an intrinsic pulse width.

When no evidence was found for either an intrinsic burst width or scattering, I set upper limits on their values by evaluating the posterior distribution for Model 3 with the scattering frequency-dependency index set at $\alpha = 4$.

2.3 Results

I begin by walking the reader through the fitting process for FRB 110220, which was modelled by Thornton et al. (2013) with a Gaussian profile convolved with an exponential scatter-broadened profile. By eye, Models 0 and 1 are inconsistent with the data; this was confirmed by exceedingly high BICs for these models. A fit of Model 2 to the data resulted in a value of $\alpha = 3.6 \pm 0.5$, which is consistent to within the error range with the Thornton et al. (2013) value of 4.0 ± 0.4 . It is difficult to compare my value of $\tau_{1\text{ GHz}} = 11.4 \pm 0.4$ ms with the width at 1.3 GHz estimated by Thornton et al. (2013) (5.6 ± 0.1 ms), given differences in the fitted models and the measurement uncertainties. Finally, to check whether any intrinsic width is detectable, I conducted a fit of Model 3 to the data with α set to a value of 4. The estimated posterior densities for this model are shown in Fig. 1. It is evident both from the shape of the marginalised posterior distribution in ζ , and from a comparison of the BICs between Models 2 and 3 (the BIC for Model 3 was three units greater than the BIC for Model 2) assuming the best-fitting parameters, that there is no evidence for an intrinsic width besides the DM-smearing timescale. This result is also consistent with the findings of Thornton et al. (2013).

Fig. 1 also serves to illustrate the levels of covariances

that I typically found between model parameters. These are negligible. The scattering timescale, $\tau_{1\text{ GHz}}$, is most covariant with other parameters, in particular t_0 and c_1 .

I show fits to data on thirteen of the Parkes FRB sample in Fig. 2; details of the specific models and best-fit parameters are given in Table 2. I show temporal profiles averaged over the upper and lower halves of the respective observing bands (§2.1), after rejection of channels 0–160 in the case of BPSR. I dedispersed the data using the DMs from the original analyses of the FRBs (DM_{init}); in some cases, significantly different DMs were derived (e.g., FRB 010724; Fig. 2 top-right panel). I do not show the results for FRBs 131104 and 150807, because they have been previously fit using my technique (Ravi et al. 2015, 2016). Note that in Table 2, the fluence coefficients c_i are scaled to be in units of σ_i -ms, where σ_i is the noise-floor standard deviation in channel i in one millisecond (see Table 1).

The final two Parkes FRBs that are excluded from Fig. 2, 121002 and 130729, could not be modelled using any of Models 0–3. These FRBs are also excluded from Table 2. This is because they both exhibit two temporal components. I show the dedispersed dynamic spectra of these FRBs in Fig. 3. Interesting spectral structure is also present in FRB 130729, which appears concentrated in the lower part of the observing band.

2.3.1 Notes on individual FRBs

FRB 010125: Burke-Spolaor & Bannister (2014) found a width for this FRB of $\zeta \approx 5$ ms, in excess of the DM smearing timescale, although it was unclear from their analysis whether this was intrinsic to the pulse or caused by scattering. By analysing the variation with frequency of the pulse width, they claim a detection of scattering with $\alpha = 4.2 \pm 1.2$. This is also consistent with $\alpha = 3$, which would simply correspond to a DM-smearing pulse, as they did not appear to account for DM smearing in their analysis of the frequency-variation of the pulse width. My analysis suggests that this was indeed the case: I find no evidence for temporal structure in FRB 010125 besides DM smearing (Model 0).

FRB 010621: In agreement with Keane et al. (2012), the present analysis reveals no evidence for temporal structure in this FRB besides DM smearing. Although the Galactic disk DM contribution along this low-Galactic-latitude sightline is expected to be 534 pc cm^{-3} , the expected scattering timescale is only $\tau_{1\text{ GHz}} = 0.15$ ms (Cordes & Lazio 2002); this is well below our upper limit of $\tau_{1\text{ GHz}} < 3.9$ ms (95% confidence).

Through an analysis of velocity-resolved H α and H β observations of the Galactic interstellar medium (ISM) along the burst sightline, Bannister & Madsen (2014) concluded that previous estimates for the Galactic disk DM contribution were underestimated, and that this burst is in fact Galactic (90% confidence). A potential problem for this hypothesis is my upper limit on the scattering timescale. Bannister & Madsen (2014) predict a scattering timescale of

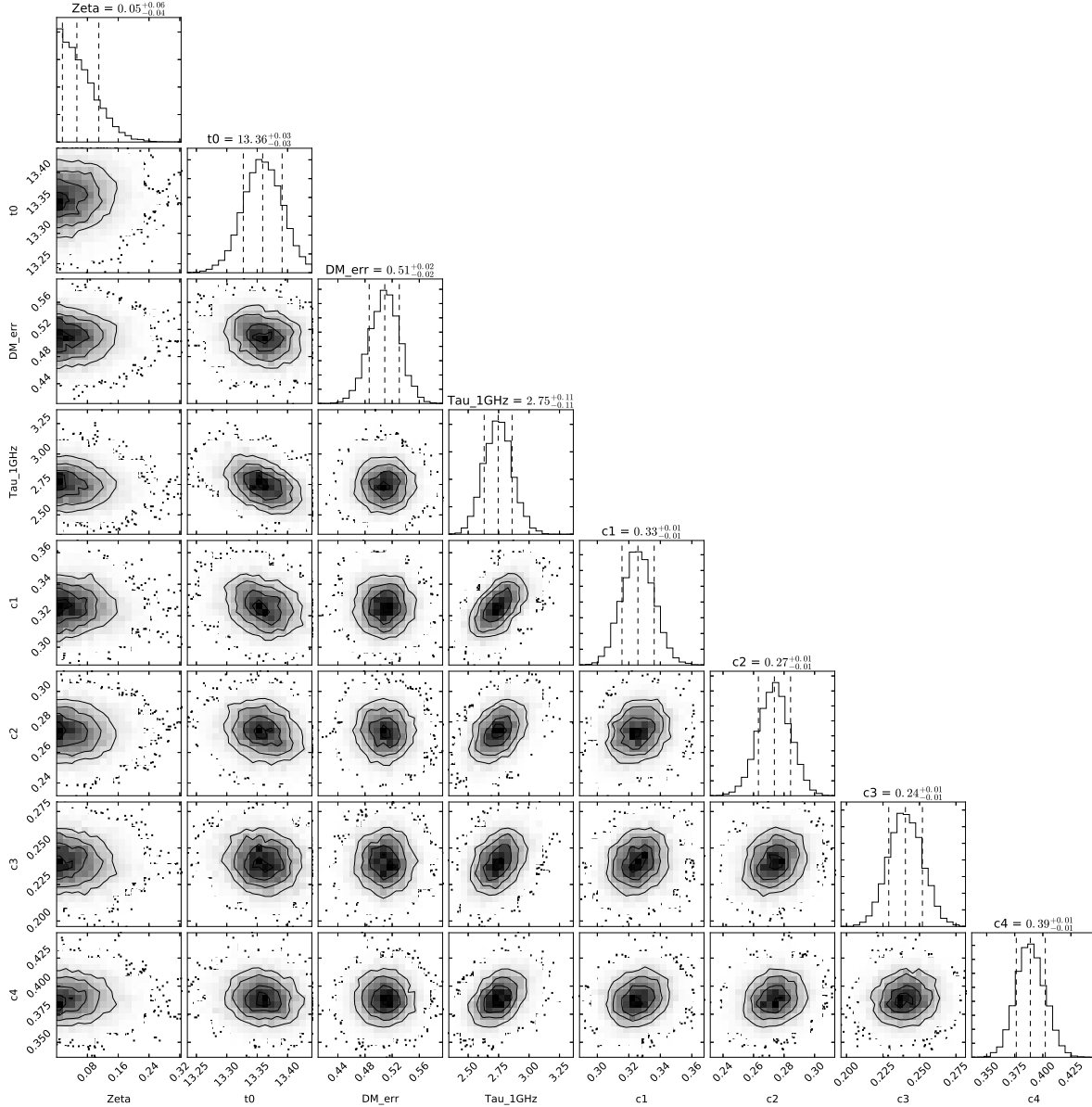


Figure 1. Posterior density estimates for a fit of Model 3 to data for FRB 110220, assuming $\alpha = 4$. The parameters of the fit were ζ (Zeta), t_0 (t_0), DM_{err} (DM_{err}), $\tau_{1\text{GHz}}$ ($\text{Tau}_{1\text{GHz}}$), and c_1 to c_4 ($c_1 - c_4$). Estimated marginalised posterior densities in each parameter are shown as histograms of samples of the posterior, and joint densities between all pairs of parameters are shown by shading and contours. 48000 samples of the posterior were obtained.

≈ 2.4 ms in the observing band, corresponding to $\tau_{1\text{GHz}} \approx 8.5$ ms, which is excluded by my upper limit. On the other hand, the relation between DM and $\tau_{1\text{GHz}}$ in the Galaxy has a large intrinsic scatter (0.76 dex; Cordes et al. 2016). Nonetheless, for a Galactic sightline with the DM of the burst (746 pc cm^{-3}), the burst would have to be under-scattered by a factor of $\approx 2.5\sigma$. This could be because significant amounts of DM are contributed by higher-density gas surrounding the source or hot ISM with weak density fluc-

tuations, or that the scattering is dominated by localised clumps rather than the bulk ISM (Cordes et al. 2016).

FRB 010724: I find moderate evidence for both an intrinsic width and an exponential scattering “tail” in this FRB. The present analysis differs from that of Lorimer et al. (2007) because it uses the sum of data from the three non-saturated beams, rather than data from the saturated beam alone. Nonetheless, my estimates of the scattering timescale, $\tau_{1\text{GHz}} = 25 \pm 5$ ms, and index, $\alpha = 6.4 \pm 1.7$, are consis-

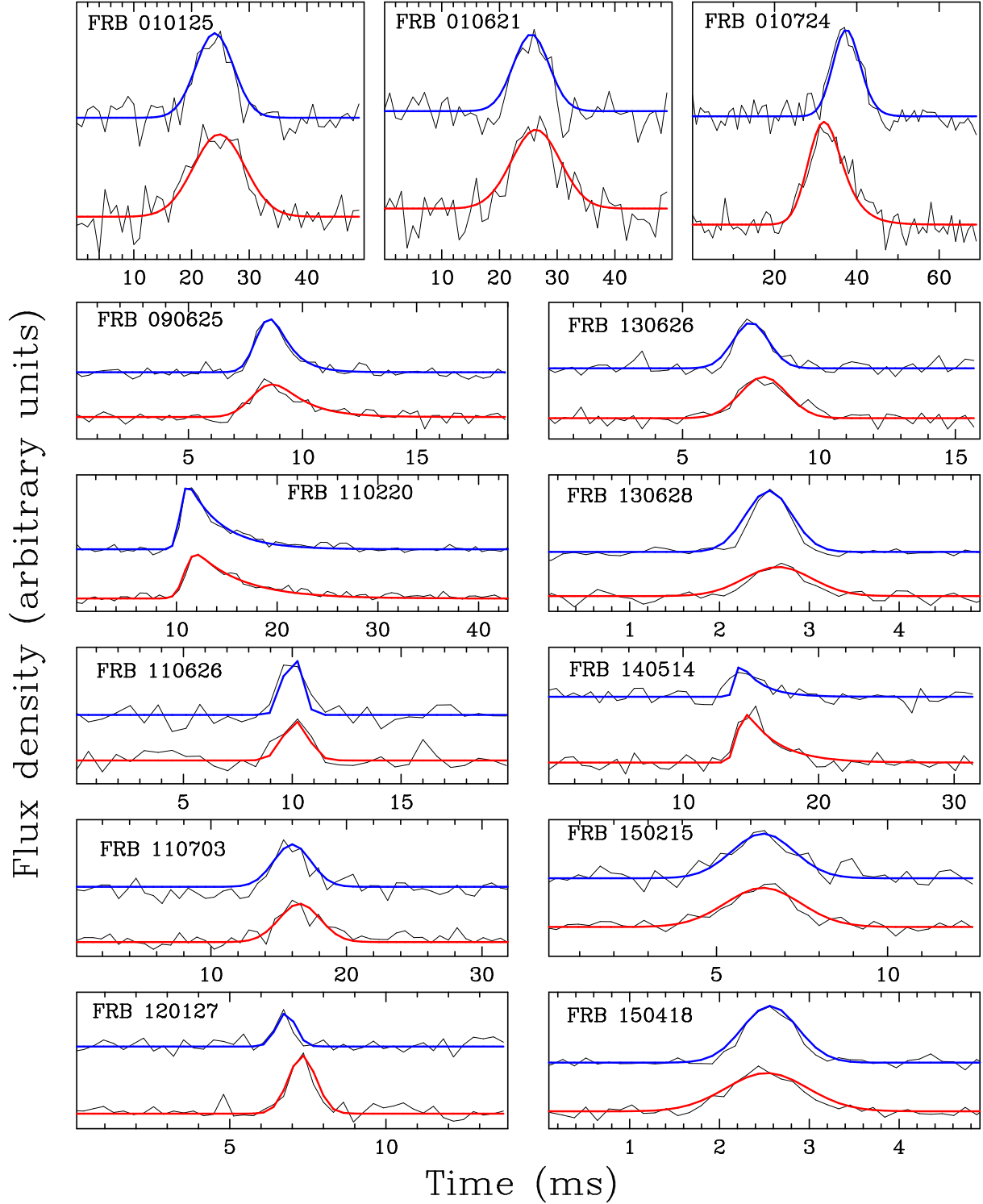
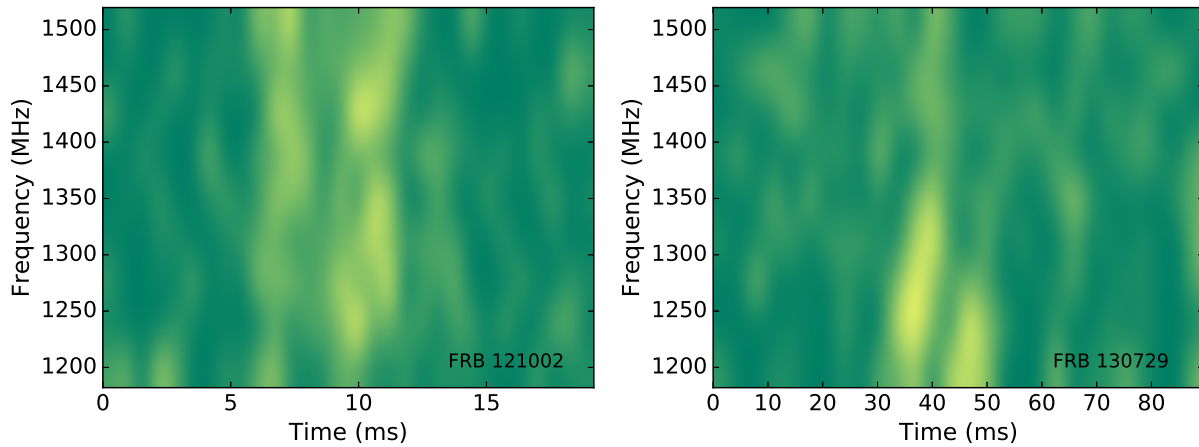


Figure 2. Data (thin black lines) and model fits (thick blue and red lines) for a selection of FRBs. In each panel, the top and bottom curves (corresponding to the blue and red dashed lines respectively) are the mean temporal profiles of the FRBs in the upper- and lower-frequency halves of the observing bands, respectively. The relative flux-density scales between the temporal profiles in the two bands are normalised to the respective noise levels; the uniform frequency-response of the Parkes multibeam system implies that the temporal profiles in the two bands are on approximately the same absolute amplitude scale. Details of the exact bandwidths are given in the text, and details of the model fits are presented in Table 2.

Table 2. FRB properties. Errors in the last significant figures are given in parentheses.

FRB	DM (pc cm ⁻³)	$\tau_{1\text{ GHz}}$ (ms)	α	ζ (ms)	c_1 (σ_1)	c_2 (σ_2)	c_3 (σ_3)	c_4 (σ_4)	Best model
010125	792.3(1)	< 9.6	–	< 1.25	38(4)	54(5)	56(4)	76(5)	0
010621	745.9(2)	< 3.9	–	< 1.4	36(4)	31(4)	42(5)	58(5)	0
010724	362.7(1)	25(5)	6.4(1.7)	2.4(3)	45(4)	53(4)	78(5)	75(5)	3
090625	899.14(6)	5.2(5)	4(1)	< 0.2	11.5(7)	8.2(6)	9.9(7)	6.6(7)	2
110220	944.83(5)	11.4(4)	3.6(5)	< 0.2	63(2)	53(2)	48(2)	76(2)	2
110626	723.3(4)	< 0.57	–	< 0.46	4.5(7)	5.1(6)	5.2(9)	4(1)	0
110703	1104.1(5)	32(1)	–	< 0.71	8(1)	20(2)	19(2)	12(2)	2
120127	554.22(3)	< 1.53	–	< 0.18	1.1(3)	1.9(3)	3.2(4)	4.8(4)	0
130626	952.01(5)	2.8(4)	–	< 0.52	5.1(5)	5.3(5)	6.6(6)	5.8(7)	2
130628	469.98(1)	< 0.23	–	< 0.04	2.4(1)	2.1(1)	1.8(1)	1.5(2)	0
131104	778.5(1)	15(2)	4.4(8)	< 0.18	11.9(6)	12.5(6)	10.5(6)	8.0(6)	2
140514	563.8(6)	< 6.1	–	1.2(1)	7(1)	8(1)	14(1)	16(1)	1
150215	1106.8(3)	< 0.47	–	0.7(1)	6.1(7)	5.7(7)	7.0(8)	5.6(7)	1
150418	775.84(1)	0.12(1)	–	< 0.05	1.37(6)	1.44(7)	1.57(7)	1.30(8)	2
150807	266.5(1)	< 0.08	–	< 0.04	1.1(1)	3.58(9)	12.6(1)	12.1(1)	0


Figure 3. Dedispersed dynamic spectra of FRBs 121002 (left) and 130729 (right), for which Models 0–3 were insufficient. In both cases, two temporal components are evident. The dynamic spectra have been interpolated using a bicubic spline fit. As with Fig. 2, the data in each spectral channel have been normalised to the respective noise levels; the colour-scale therefore represents the signal to noise ratio (S/N) in linear units.

tent with those of Lorimer et al. (2007) (24.13 ± 3 ms and 4.8 ± 0.4 respectively). I also revise the DM estimate from 375 pc cm^{-3} to $362.7 \pm 0.1 \text{ pc cm}^{-3}$.

FRB 110703: Unlike the analysis of Thornton et al. (2013), I find moderate evidence for the presence of a significant scattering tail in this FRB ($\tau_{1\text{ GHz}} = 32 \pm 1$ ms). However, a constrained value for α cannot be determined, and I hence assume $\alpha = 4$.

FRB 130729: Like FRB 121002, this burst has two temporal components. Unlike FRB 121002, FRB 130729 also has a discontinuous spectrum (Fig. 3), with most power concentrated in the lower part of the band. It is unclear whether the scattering timescale derived by Champion et al. (2016) for this FRB is real, or is attributable to the unusual temporal and spectral structure.

FRB 130628: Unlike Champion et al. (2016), I find no evidence for a scattering tail in this FRB, or for any structure beyond that described by Model 0. Indeed, my upper limit on the scattering timescale, $\tau_{1\text{ GHz}} < 0.23$ ms, is well below the previous estimate of $\tau_{1\text{ GHz}} = 1.24 \pm 0.07$ ms.

FRB 140514: For this FRB, Models 1 and 2 had equivalent BICs. I hence choose Model 1 for this FRB, and thus do not find any evidence for the existence of scattering, unlike Petroff et al. (2015). Along with FRBs 121002 and 130729, this is one of the few FRBs to exhibit temporal structure beyond Model 0 with no clear evidence of scattering. It also has a mildly inhomogeneous spectrum, as indicated by the c_i coefficients in Table 2.

FRB 150215: In agreement with Petroff et al. (2017),

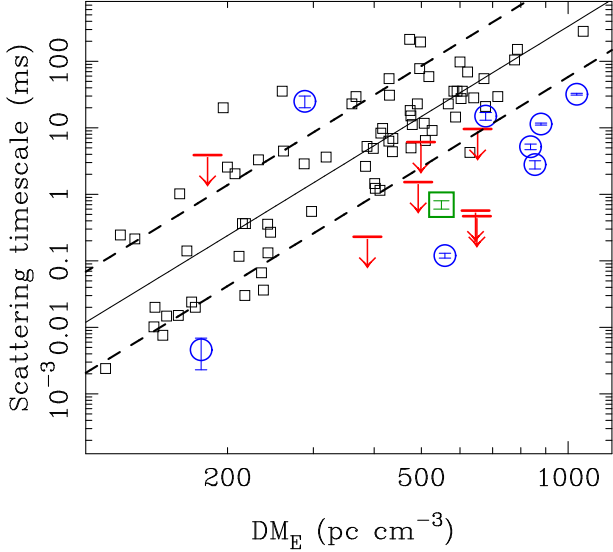


Figure 4. Measurements of DM_E and $\tau_{1\text{GHz}}$ for FRBs in Table 2: cases where $\tau_{1\text{GHz}}$ is measured are shown as blue circles with error-bars, and upper-limits on $\tau_{1\text{GHz}}$ are indicated by downward-facing red arrows. I also show measurements for the Green Bank Telescope FRB 110523 (Masui et al. 2015) as a large green square. The solid and dashed lines indicate the Galactic $\tau_{1\text{GHz}}$ -DM relation and its intrinsic scatter, respectively, derived by Cordes et al. (2016). The black squares show pairs of measurements of DM and $\tau_{1\text{GHz}}$ for Milky-Way pulsars from the ATNF pulsar catalogue (Manchester et al. 2005). All pulsars with published measurements of $\tau_{1\text{GHz}}$ are included here.

I find evidence for a larger temporal width than is expected in Model 0, which appears to be intrinsic to the burst.

FRB 150418: In contrast to the analysis of Keane et al. (2016), I find that this FRB exhibits a weak scattering tail, with a timescale of $\tau_{1\text{GHz}} = 0.12 \pm 0.01$ ms. The value of α cannot be constrained.

FRB 150807: This FRB was modelled using similar techniques by Ravi et al. (2016). No evidence was found for any temporal structure beyond Model 0 in either the previous or present analysis. Although I present an upper limit on $\tau_{1\text{GHz}}$ in Table 2, in the analysis below I use the value inferred from the frequency-scintillations of $1.6 \pm 0.8 \mu\text{s}$ (Ravi et al. 2016) at 1.3 GHz, corresponding to $\tau_{1\text{GHz}} = 4.6 \pm 2.3 \mu\text{s}$.

2.4 Astrophysical implications

As foreshadowed in the Introduction, an immediate utility of my quantitative results is to investigate the scattering strengths of FRBs at different DMs. I have only marginally adjusted the FRB DMs, and, as shall be shown in the following section, the fluence constraints for most FRBs are not tight enough to enable a rigorous analysis of the distribution of FRB fluences.

A relationship between the scattering timescale, $\tau_{1\text{GHz}}$, and DM is firmly established for Milky-Way pulsars over

three orders of magnitude in DM, and eleven orders of magnitude in $\tau_{1\text{GHz}}$. The large intrinsic scatter of 0.76 dex, and the steeper slope of the relation at $DM \gtrsim 100$, are interpreted as evidence for clumpiness in the ionised ISM (Cordes et al. 1991, 2016). Motivated by the strong evidence for scattering in FRB 110220 presented by Thornton et al. (2013), the possibility of a $\tau_{1\text{GHz}}$ -DM relation existing for FRBs putatively scattered in the intergalactic medium (IGM) was first considered by Lorimer et al. (2013). However, the possibility of any significant scattering in the IGM was disputed by Macquart & Koay (2013) and Luan & Goldreich (2014), based on their assessments of IGM turbulence.

The existence of a $\tau_{1\text{GHz}} - DM_E$ relation for FRBs, where DM_E is the estimated extragalactic DM component for a given FRB, would thus imply that FRBs are predominantly scattered in the ionised medium that dominates the DM_E values. For example, if DM_E is typically dominated by contributions from the IGM, it would be possible that FRBs are predominantly scattered in the IGM or in intervening bound systems. On the other hand, if DM_E is typically dominated by host-galaxy contributions, a $\tau_{1\text{GHz}} - DM_E$ relation would reflect the typical DM- $\tau_{1\text{GHz}}$ relation in FRB host galaxies. The lack of a $\tau_{1\text{GHz}} - DM_E$ relation would imply that the medium that dominates the DM_E -values does not significantly scatter FRBs.

Cordes et al. (2016) compared existing measurements of FRB scattering timescales with a revised $\tau_{1\text{GHz}}$ -DM relation for Milky-Way pulsars. No evidence was found for a $\tau_{1\text{GHz}} - DM_E$ relation for FRBs. However, it was shown that FRBs are typically under-scattered in comparison to their values of DM_E , relative to Milky-Way pulsar scattering timescales at congruent values of DM. This was interpreted either as an indication that 50 – 75% of DM_E is typically contributed by the IGM, or that FRB host galaxies have ISMs that are typically less turbulent than the ISM of the Milky Way. The possibility of FRBs being predominantly scattered in the IGM was thought less likely owing to the large levels of scattering present relative to expectations for the IGM (e.g., Macquart & Koay 2013), and the lack of a $\tau_{1\text{GHz}} - DM_E$ relation.

The discovery of FRB 150807 (Ravi et al. 2016), however, significantly extended the range of FRB scattering timescales. Although not detectably temporally broadened due to scattering, this FRB exhibited frequency-scintillations that indicated a scattering strength much greater than that expected from its Milky-Way sightline (Shannon et al., in preparation). The combined measurements of low scattering and low Faraday rotation-measure indicated that this FRB was most likely not scattered in ISM with turbulence and magnetisation like that of the Milky Way. However, constraints on the distance to the source of FRB 150807 suggested that a significant portion of its DM_E originated in the IGM.

Using my revised measurements of DM and $\tau_{1\text{GHz}}$ for the Parkes FRB sample (Table 2), I plot $\tau_{1\text{GHz}}$ against

DM_E in Fig. 4. I also show measurements for FRB 110523 (Masui et al. 2015) discovered at the Green Bank Telescope in the 700-900 MHz band. For each FRB, I estimate DM_E by subtracting the maximum Galactic-disk DM predicted by the NE2001 DM model (Cordes & Lazio 2002) along the FRB sightline, and by further subtracting a contribution of 30 pc cm^{-3} corresponding to the Milky Way ionised-gas halo and the Local Group (e.g., Gupta et al. 2012; Dolag et al. 2015). In Fig. 4, I also plot the Milky Way $\tau_{1 \text{ GHz}}\text{-DM}$ relation derived most recently by Cordes et al. (2016), and pairs of measurements of $\tau_{1 \text{ GHz}}$ and DM for Milky-Way pulsars from the ATNF pulsar catalogue (Manchester et al. 2005).

First, Fig. 4 supports the finding of Cordes et al. (2016) that FRBs are under-scattered with respect to their values of DM_E . This is despite the differences in the actual measurements, and in the compositions of the samples, between the two analyses. Relative to the Cordes et al. analysis, I discard FRBs 121002 and 130729 due to their complex temporal and spectral structures, which may have biased previous scattering measurements, but include the new FRB 150807 and its value of $\tau_{1 \text{ GHz}}$ based on the frequency-scintillations. The exclusion of FRBs 121002 and 130729 may bias inferences from Fig. 4, because our ability to discern the complex temporal structure relies on them not being strongly scattered. However, any upper limits that could be placed on their scattering timescales would correspond approximately to the narrowest features in the burst profiles (i.e., a few milliseconds at $\sim 1.3 \text{ GHz}$; see Fig. 3). These in turn would be approximately consistent with existing measurements in Fig. 4.

Fig. 4 provides tentative indications of a relation between $\tau_{1 \text{ GHz}}$ and DM_E for FRBs similar to that for Milky-Way pulsars. If FRB 010724, which has the largest $\tau_{1 \text{ GHz}}/DM_E$ ratio among the FRB sample, is excluded, the $\tau_{1 \text{ GHz}} - DM_E$ relation appears somewhat stronger. Using the BIC, I quantify the evidence for a $\tau_{1 \text{ GHz}} - DM_E$ relation by comparing linear models for the DM_E and $\tau_{1 \text{ GHz}}$ measurements, with, and without, a dependency of $\tau_{1 \text{ GHz}}$ on DM_E . Consider the log-likelihood function

$$L = \sum_i \left[-\log(\epsilon_i^2 + \epsilon^2) - \frac{(\log_{10} \tau_{1 \text{ GHz},i} - M_i)^2}{2(\epsilon_{M,i}^2 + \epsilon^2)} \right] \quad (6)$$

where $M_i = m \log_{10} DM_{E,i} + b$ is a log-linear model for the $\tau_{1 \text{ GHz}} - DM_E$ relation with parameters m and b and intrinsic scatter ϵ , and $DM_{E,i}$ and $\tau_{1 \text{ GHz},i}$ are FRB measurements indexed by i with error ϵ_i . I consider the difference in BIC between the maximum of this likelihood function in the parameters m , b and ϵ , and the maximum of the likelihood function with a fixed $m = 0$ (and hence one less parameter). With the sample of eight Parkes FRBs with measurements of $\tau_{1 \text{ GHz}}$, there is no significant difference in the BICs between the two models. However, with FRB 010724 excluded, the difference in BICs is 8, which I consider moderately significant. The inclusion of the upper-limits on scattering timescales does not significantly alter these results. For the seven-FRB sample (excluding FRB 010724), I find $m = 7 \pm 2$

and $b = -19 \pm 5$; I emphasise that these results are likely to change significantly as more scattered FRBs are discovered.

A $\tau_{1 \text{ GHz}} - DM_E$ relation for FRBs is would not be particularly surprising, because it would simply imply that significant portions of FRB DMs are contributed by a class of medium that has a scattering strength which scales with its column-density. It is well-established that the Milky Way ISM is one such class of medium. It is generally thought to be unlikely that FRBs are predominantly scattered in the Milky Way itself, because they would lie along sightlines of intolerably large $\tau_{1 \text{ GHz}}$ for the Milky-Way DM contributions. If FRBs were, however, scattered in host galaxies like the Milky Way, approx. 75% of the typical FRB DM must be contributed by an IGM that has a weak potential for scattering. This is difficult to reconcile with the results on FRB 150807 (Ravi et al. 2016). Note further that in this case a fair comparison between the Milky-Way $DM\text{-}\tau_{1 \text{ GHz}}$ relation and FRB measurements would require the values of $\tau_{1 \text{ GHz}}$ for Milky Way sightlines to be scaled up by a factor of three (Cordes et al. 2016), to account for the difference in scattering geometry between the Milky Way (presumably a homogeneous scattering medium along the line of sight), and FRBs scattered in host galaxies (scattering medium concentrated around the FRBs). Alternatively, FRBs may instead be scattered in the IGM, or in intervening bound systems, and experience negligible host-galaxy scattering. An attempt to ascertain the necessary properties of scattering regions in the IGM and intervening systems is beyond the scope of this work. The different scenarios for FRB scattering will be tested when multiple scattered FRBs are localised to individual host galaxies, and their distances thus measured, such that the host and IGM contributions to the DM may be separately estimated. In any scenario for the dominant contributor of FRB DMs, a $\tau_{1 \text{ GHz}} - DM_E$ implies that more (cosmologically) distant FRBs will be more difficult to detect.

3 FRB FLUX DENSITIES

Here, I quantify the constraints that may be placed on FRB fluences based on an analysis of the Parkes MBR sky-response. In §3.1, I consider what constraints may be placed on the flux densities of FRBs detected in individual beams of the MBR. Then, in §3.2, I constrain the location of the multiple-beam FRB 010724 in the Parkes focal plane using a technique similar to that applied by Ravi et al. (2016) to the dual-beam FRB 150807. Third, in §3.3, I combine these analyses with the fluence estimates presented in Table 2, and compare the resulting FRB fluence constraints with various specifications for the FRB fluence distribution (the logN-fluF).

3.1 Single-beam FRBs

The exact locations of single-beam FRBs within the sky-response functions of the beams, $\Theta(\theta, \phi)$, are unknown. Here,

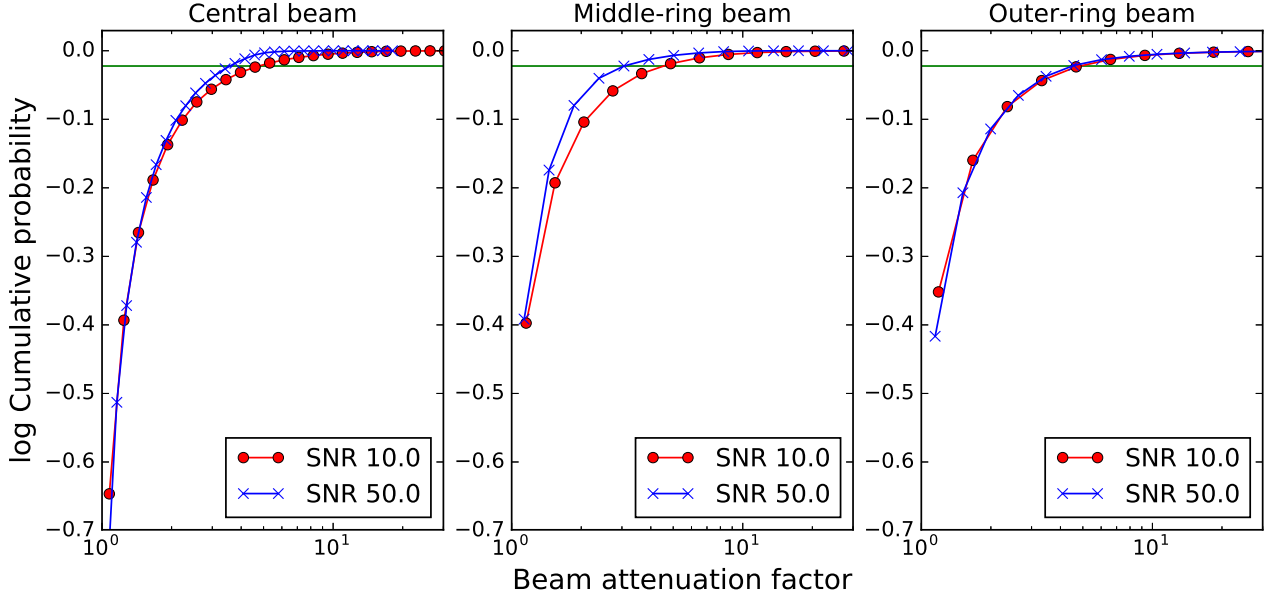


Figure 5. The cumulative probabilities, $P(> \Theta)$, for FRBs being detected above different beam attenuation factors, Θ (see text for details). From left to right, I show results for the central, an inner-ring, and an outer-ring beam of the Parkes MBR. I consider FRBs detected with S/N of 10 (red line with filled circles) and 50 (blue line with crosses). The horizontal green lines indicate the 95th percentiles of the distributions.

$\Theta(\theta, \phi)$ is the attenuation of the FRB due to an off-axis position at polar coordinates, (θ, ϕ) , in the focal plane; for an on-axis feed, $\Theta(\theta, \phi)$ may be well-approximated by the inverse of an Airy function. That is, the beam attenuation factor is the inverse of the standard beam gain pattern. By adopting models for $\Theta(\theta, \phi)$ for the Parkes receiver, and for the distribution of FRB fluences, it is possible to evaluate the probable beam-attenuations of FRBs detected in different beams.

I used the model for $\Theta(\theta, \phi)$ for the Parkes MBR presented by Ravi et al. (2016). This analytic model was found to be consistent with measurements at the -20 dB response level. For each beam, I used the model to evaluate $\Theta(\theta, \phi)$ on a grid of 1000×1000 points spanning 3×3 deg in θ and ϕ . I averaged the model in frequency across the BPSR band (1182 – 1519.5 MHz); I did not find the results in this section to vary significantly when instead using the AFB band. Then, for the central, an inner-ring, and an outer-ring beam, I derived the histograms of pixel-values of $\Theta(\theta, \phi)$ where the FRB would not be detected with $S/N > 3$ in any other beam; I considered S/Ns of 10 and 50 in the primary detection beams. These histograms provided initial estimates of the probability density functions of Θ for FRBs detected in individual beams of the MBR.

However, FRBs are not equally likely to be detected at different fluences or flux-densities³: the specific distribution

in these parameters is the logN-logF function. For a fluence F , the number of FRBs expected at fluences $> F$ is typically modelled as a power-law: $N(> F) \propto F^{-\beta}$, for some power-law index β (e.g., Vedantham et al. 2016). For a uniform distribution of FRBs in Euclidean space, $\beta = 1.5$. However, based on the unexpected detection of multiple-beam FRBs at Parkes (FRBs 010724 and 150807), Vedantham et al. (2016) showed that the Parkes FRB sample is consistent with $0.5 < \beta < 0.9$ (90% confidence). I therefore adopted $\beta = 0.7$, and scaled the Θ -histogram counts accordingly. Finally, I used the histograms to derive the probabilities of detecting FRBs above given values of Θ (Fig. 5).

From Fig. 5, it is apparent that single-beam FRBs in any beam are most likely to be detected with $\Theta < 5$ ($> 95\%$ confidence for $S/N \gtrsim 50$). They are expected to be detected with $\Theta < 2$ with $\approx 80\%$ confidence, suggesting that the conventionally quoted FRB localisation accuracy of the FWHM of the primary beam (e.g., Petroff et al. 2015; Keane et al. 2016) is only moderately efficacious. If the slope, β , of the FRB logN-logF function were larger(smaller), the maximum likely value of Θ would decrease(increase). For higher-significance FRBs, the maximum likely value of Θ would also decrease, although only marginally so for FRBs detected in outer-ring beams.

3.2 FRB 010724 (the Lorimer burst)

As discussed above, FRB 010724 was detected in four beams of the Parkes MBR: the inner-ring beams 6 and 7, and

³ In this context, fluence and flux density can be used interchangeably.

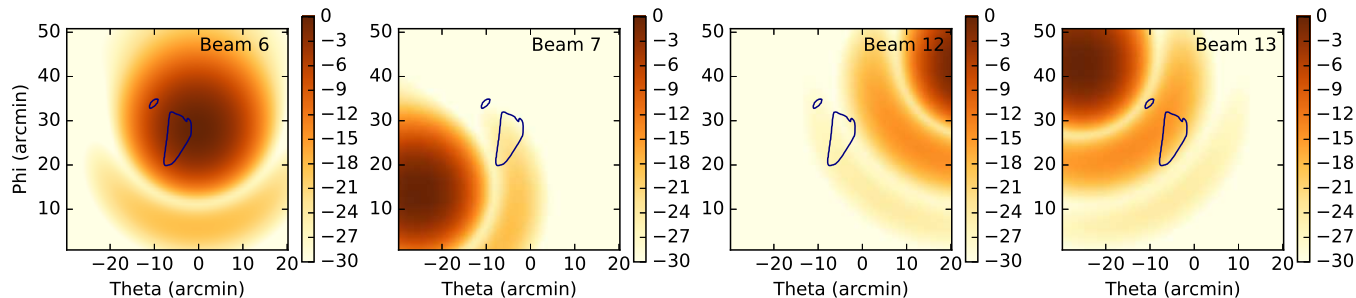


Figure 6. The 99% confidence containment region of FRB 010724 (blue contours) shown relative to the sky-response functions of beams 6, 7, 12 and 13 of the Parkes MBR. The colour-bars indicate the beam attenuation factors, $\Theta(\theta, \phi)$, at different positions in the Parkes focal plane, in units of decibels.

the outer-ring beams 12 and 13. Following the technique of Ravi et al. (2016), I use the relative S/Ns of the burst in the different beams, and a model for the individual sky-response functions of the beams, to constrain the position of the burst in the Parkes focal plane. This in turn provides a constraint on the flux-density of the burst. I defer an analysis of the localisation region on the sky of FRB 010724 to a future paper.

FRB 010724 saturated the one-bit AFB digitiser for beam 6, making it impossible to accurately measure the S/N in this beam. Accurate measurements are however possible for beams 7, 12 and 13. After averaging the data for these beams over the AFB band, I smoothed each time-series with a top-hat function of width 6 ms, and estimated the peak S/N in each beam. I ensured that the peak S/N in each beam occurred at the same time. For beams 7, 12 and 13, the S/Ns were 13.9, 5.5 and 22.1 respectively. Unlike the analysis of FRB 150807 by Ravi et al. (2016), I did not attempt to use measurements at multiple frequencies because of the relatively weak detections in these three beams.

I evaluated models for the sky-response functions of each beam, averaged over the AFB band, using the publicly-available codes presented by Ravi et al. (2016). The models were evaluated, as above, on a grid of 1000×1000 points spanning 3×3 deg in the Parkes focal plane. I then made Monte Carlo realisations of the S/N in each beam, based on the estimated S/Ns, to calculate a containment region. For each realisation, I found points in the focal plane where the ratios of S/Ns between beams 7, 12 and 13 were within a factor of four of the simulated measurements. I accounted for the difference in telescope gain between inner- and outer-ring beams. I rejected points where the burst would have been detected with $S/N \geq 3$ in any of beams 1, 2, 3, 4, 5, 8, 9, 10 and 11, and also rejected points where the burst would have been detected with a lower S/N in beam 6 than in any other beam. Finally, I averaged the results over 1000 realisations. I note that this analysis places no prior on the $\log N$ - $\log F$ function, unlike the analysis in §3.1.

In Fig. 6, I show the resulting 99% confidence containment region for FRB 010724 in the Parkes focal plane. The

localisation is to approx. 50 arcmin^2 . This is substantially worse than the 9-arcmin^2 localisation of FRB 150807. This is most likely because I do not use measurements at different frequencies for FRB 010724, whereas measurements in four sub-bands were used to localise FRB 150807.

The results suggest that the S/Ns in beams 7, 12 and 13 should be scaled upwards by factors of 310 ± 180 , 510 ± 140 and 80 ± 40 , respectively. Based on the S/N measurements, the fluence measurements for FRB 010724 in Table 2 should thus be scaled upwards by factor of 200 ± 100 . Assuming gains of 1.45 Jy K^{-1} and 1.72 Jy K^{-1} for the inner- and outer-ring beams, a common system temperature of 28 K (Manchester et al. 2001), and a one-bit digitisation loss factor of 1.25 (Keane & Petroff 2015), the mean fluence of FRB 010724 within the AFB band is $(800 \pm 400) \text{ Jy ms}$.

3.3 Astrophysical implications

The best utility of my revised fluence constraints for the Parkes FRB sample is to consider the implications for the $\log N$ - $\log F$. I use the fluence estimates in Table 2 for all FRBs besides 010724 and 150807, averaged over the frequency bands, and the sensitivity parameters given above, to derive minimum fluences for each FRB assuming bore-sight positions in the detection beams. Using the results summarised in Fig. 5, I also derive 95% confidence fluence upper limits for each FRB. For FRBs 010724 and 150807, I use the constrained 1σ fluence ranges that were derived above in §3.2 and by Ravi et al. (2016) respectively, enabled by their multiple-beam detections. I collate the fluence measurements to derive lower- and upper-limiting empirical $\log N$ - $\log F$ distributions, which are displayed in Fig. 7.

In the Figure, I also show various $\log N$ - $\log F$ functions of index -0.7 , which was the value inferred by Vedantham et al. (2016), and of index $-3/2$, which corresponds to a uniform distribution of sources in Euclidean space. In comparing the empirical distributions with the assumed intrinsic power-law $\log N$ - $\log F$ functions, a number of selection effects must be recognised. First, the data in Fig. 7 are comprised of FRBs detected with both the BPSR

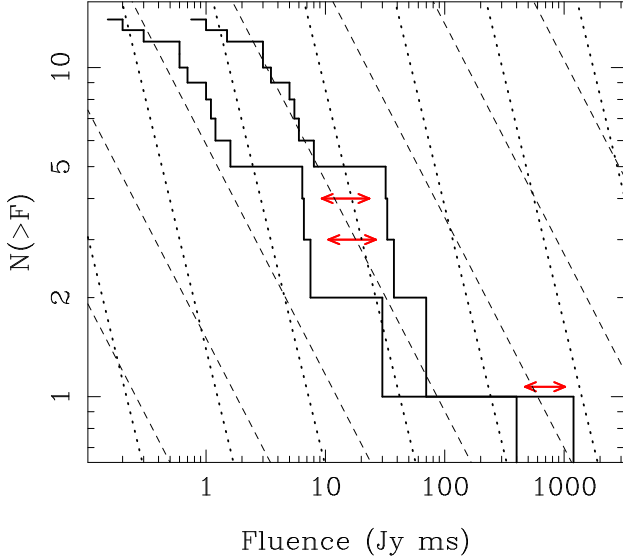


Figure 7. Empirical logN-logF distribution for the Parkes FRB sample that I model herein. The lower-fluence binned trace indicates the minimum fluence values for each FRB, and the higher-fluence binned trace indicates the maximum fluence values for each FRB. The minimum fluences are derived assuming boresight positions in the detection beams for most FRBs, and the lower bounds on the 1σ fluence ranges for FRBs 010724 and 150807. The maximum fluences are the 95% confidence upper limits on the fluences for most FRBs derived using the results in Fig. 5, and the upper bounds on the 1σ fluence ranges for FRBs 010724 and 150807. The dashed lines indicate logN-logF functions proportional to $F^{-0.7}$ (Vedantham et al. 2016), and the dotted lines indicate logN-logF functions proportional to $F^{-3/2}$. Although the fluence upper-bounds derived using Fig. 5 assume a logN-logF function proportional to $F^{-0.7}$, the higher-fluence binned trace would simply be shifted lower or higher in fluence for steeper or flatter logN-logF functions, respectively. The horizontal red arrows indicate the FRBs detected with the AFB.

and AFB instruments; FRBs detected with the AFB are indicated by red arrows. The differing sensitivities of these instruments, attributable to different numbers of bits in the analogue-to-digital conversion, the different bandwidths, and different integration times, mean that the instruments are fluence-incomplete (Keane & Petroff 2015) below different thresholds. This threshold is $\approx 2 \text{ Jy ms}$ for BPSR, and $\approx 3 \text{ Jy ms}$ for the AFB. Second, it is possible that the FRB rate varies with Galactic latitude (Petroff et al. 2014; Burke-Spolaor & Bannister 2014). Certainly, different sky radiation-temperatures result in different sensitivities for different pointings. The combination of FRB detections from varied searches, even with the BPSR instrument, may therefore result in a biased estimate of the sky-averaged FRB logN-logF function. Given these issues, and factor of ~ 5 uncertainty in the flux-density values, I concur with Keane & Petroff (2015) and Vedantham et al. (2016) that it is not useful to attempt to use the fluence measurements to directly estimate the FRB logN-logF.

4 TYPE I, TYPE II ... TYPE N FRBS

In this paper, I have focused on the Parkes FRB sample to attempt to ensure a consistent sample selection in my analysis. This is possible in particular with those FRBs detected with the BPSR instrument at Parkes. However, even within the sample of FRBs detected with BPSR, a distinction may be made between those FRBs that are consistent with the simple temporal structures in my Models 0–3, and the more complex structures seen in FRBs 121002 and 130729. Another distinction may be made between those Parkes FRBs that show signatures of scattering at levels stronger than expected from their passage through the Milky Way, and those that do not. In a broader context, the repeating nature of FRB 121102 is, *prima facie*, unique among FRBs. In this section, I explore a selection of arguments relating to the number of possible FRB source classes. Unfortunately, it appears difficult at present to distinguish between an entirely homogeneous population of FRB sources, FRB sources that are physically similar but which vary in their emission properties, and multiple independent populations of FRB sources.

4.1 A single FRB population?

A unified class of FRB emitters must fulfil the following: (a) they must be able to emit pulses at frequencies between 700 MHz (Masui et al. 2015) and 5 GHz (Marcote et al. 2017), (b) they may lie behind plasma regions with either significant or minor scattering strength, and (c) they must be capable of producing multiple pulses with a variety of morphologies and luminosities that vary by a few orders of magnitude. Neutron stars, for example, are capable of producing such a diversity of radio-emission properties, although they have not yet been empirically associated with radiation at the luminosities ascribed to FRBs.

The large quantity of follow-up observations of the Parkes FRB sample (Lorimer et al. 2007; Ravi et al. 2015; Petroff et al. 2015; Ravi et al. 2016) implies that their characteristic repeat rate is substantially lower than that of FRB 121102. Twelve FRBs from the Parkes sample have been re-observed for a total of 340 h with identical instrumentation to the detection observations. As no repeat bursts were detected, the 95% confidence upper limit on the number of repeat bursts expected in this time is three (Gehrels 1986). Assuming that repeat bursts within a factor of 1.5 in S/N of the original events could have been detected, the 95% confidence upper limit on the rate of such repeats for the Parkes FRBs is 0.009 h^{-1} . This is substantially smaller than the rate of FRB 121102 repeats within a factor of 1.5 of the peak S/N, which, assuming that 3/17 of the repeats fulfil this criterion (Spitler et al. 2016; Scholz et al. 2016), is $\approx 0.06 \text{ h}^{-1}$. Therefore, if all FRBs were similar to FRB 121102, this object is an outlier with respect to its repeat rate, or its pulse-fluence distribution, or both.

Additionally, if all FRBs share a common class of emitter with no significant variation in the emission properties

across the population, the flat FRB logN-logF (Caleb et al. 2016; Vedantham et al. 2016) suggests that the emitter population is not uniformly distributed in the local Universe. Instead, the population may evolve strongly with distance, or may be observed at sufficient distance such that cosmological effects become important in relating volume to luminosity distance. The substantial redshift of FRB 121102 (Tendulkar et al. 2017), the localisation of FRB 150807 (Ravi et al. 2016), and the large DMs of many of the Parkes FRBs (Dolag et al. 2015) are all indicative of the cosmological interpretation. In this scenario, the Arecibo telescope would be expected to be sensitive to typically more distant FRBs than Parkes, given its greater sensitivity. However, FRB 121102 has a lower redshift than may be inferred for the Parkes FRBs with substantially larger DMs, although relating extragalactic DM to distance is significantly uncertain (Dolag et al. 2015), and this is an argument based on a sample size of unity.

On the other hand, different FRB properties may be manifested by different sub-types of the same class of emitter. For example, young FRB emitters may emit frequent pulses, whereas older FRB emitters may emit pulses only sporadically. Neutron stars, for example, exhibit such evolution in their pulse-emission properties. In this case, with respect to modelling of the FRB logN-logF, the older emitter population would be considered independent from the younger population, because the intrinsic pulse luminosity-functions of the two populations would be different. A larger variety of FRB logN-logF slopes would then be possible, for example if the older emitters could be observed at larger (cosmological) distances.

4.2 Repeating FRBs in the Parkes sample?

FRB 121102 is empirically unique among the FRB population, as it is the only known repeating source of extragalactic radio pulses. However, the question of whether it is truly unique in its class of emitter can be addressed by considering the following: given the relative amounts of time surveyed by Parkes and Arecibo for FRBs, how many more/less repeating FRBs should Parkes have detected as compared with Arecibo? Similar analyses have been conducted by Scholz et al. (2016) and Oppermann et al. (2016), who assumed that FRB 121102 and the Parkes FRBs are drawn from the same population, and thus found consistency between the detection rates at both telescopes for a uniformly-distributed, Euclidean-space population. Here I assume that repeating FRBs are uniformly distributed in Euclidean space, and calculate for each flux-density the relative number of detections above that flux density at Parkes and Arecibo.

I use the Arecibo survey details given by Scholz et al. (2016): 36.9 days searched, with a seven-beam system where each beam has an Airy-function response, $B_{\text{AO}}(\theta)$, with 3.5' FWHM. I also use the Parkes High Time Resolution Universe (HTRU) survey details given by Champion et al.

(2016): 152 days searched, with a 13-beam system where each beam has an Airy-function response, $B_{\text{PKS}}(\theta)$, with a 14.4' FWHM. To this I add the 106 days searched at Parkes by the Survey for Pulsars and Extragalactic Radio Bursts (SUPERB; Keane et al. 2017) and its successors (personal communication from E. Keane). I assume that the Arecibo system is 13.6 times as sensitive as the Parkes system (Champion et al. 2016; Scholz et al. 2016).

Note that my assumptions about the beam responses are not wholly correct, because the outer beams of both systems probe somewhat larger sky areas. This is, however, a negligible factor given other uncertainties about survey locations on the sky relative to Milky Way dispersion and scattering properties, radio-frequency interference, and the rejection of multiple-beam detections, all of which I do not include in the analysis.

For a flux density with arbitrary units given by $B_{\text{PKS}}^{-1}(\theta)$, the number of detections above this level at Parkes is proportional to

$$N_{\text{PKS}}(\theta) \propto \int_0^\theta \sin \theta' B_{\text{PKS}}^{3/2}(\theta') d\theta' \quad (7)$$

$$\times (258 \text{ days}) \times (13 \text{ beams}).$$

In the same units, and for a flux density given by $[13.6 \times B_{\text{AO}}(\theta')]^{-1}$, the number of detections above this level at Arecibo is

$$N_{\text{AO}}(\theta) \propto \int_0^\theta \sin \theta' [13.6 \times B_{\text{AO}}(\theta')]^{3/2} d\theta' \quad (8)$$

$$\times (36.9 \text{ days}) \times (7 \text{ beams}).$$

The inclusion of the effects of the telescope sky-response extends the analyses of Scholz et al. (2016) and Oppermann et al. (2016).

I plot $N_{\text{PKS}}/N_{\text{AO}}$ in Fig. 8 for different FRB flux densities, assuming FRB durations of 3 ms (corresponding to the duration of the first-detected pulse from FRB 121102) and a Parkes MBR system-equivalent flux density of 40 Jy (Keith et al. 2010). For example, if FRB 121102 always emitted 1-Jy pulses of 3-ms duration, like its first-detected pulse accounting for its detection in a primary-beam sidelobe, the fact that Arecibo has detected one such object implies that the HTRU and SUPERB surveys should expect to have detected three similar objects. If instead FRB 121102 always emitted pulses of flux-density 0.3 Jy, Parkes should expect to have detected just one such object.

The expected number of objects like FRB 121102 in the Parkes surveys, and likely within the existing sample of Parkes FRBs, depends on how the characteristic L-band flux density (or fluence) of FRB 121102 is specified. Of the repeat bursts from FRB 121102 detected at L-band with Arecibo and published by Spitler et al. (2016) and Scholz et al. (2016), only one (burst 11) likely lies above the Parkes detection threshold. It would hence have easily been possible for the first-detected burst from FRB 121102 to be below the 0.3-Jy threshold in Fig. 8 where no Parkes detections are expected given an Arecibo detection. An exact assessment of the characteristic flux density or fluence of

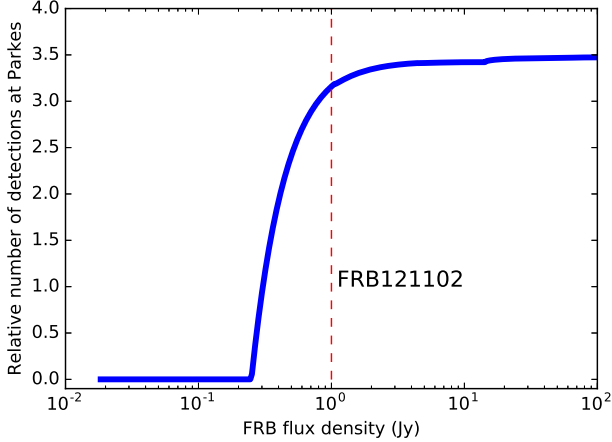


Figure 8. Number of detections of objects like FRB 121102 at Parkes above different flux densities, in the HTRU and SUPERB surveys, relative to the number of Arecibo detections. In setting the flux-density scale, I assume FRBs of 3-ms durations, like the first-detected pulse from FRB 121102; the red dashed line indicates the nominal flux density of this pulse, accounting for its sidelobe detection.

FRB 121102 requires a better determination of the distributions of these quantities among its pulses, as well as of the statistics of the temporal clustering (Spitler et al. 2016).

The effects of Galactic interstellar scintillation on this analysis are modest. The transition frequency, ν_t , between the strong and weak scattering regimes for the position of the host of FRB 121102 is $\nu_t = 37.9$ GHz (Cordes & Lazio 2002; Chatterjee et al. 2017). As the fractional diffractive scintillation bandwidth scales as $(\nu/\nu_t)^{17/5}$ (Walker 1998), the observing band at Arecibo will contain many scintles; we can hence neglect the effects of Galactic diffractive scintillation in the discovery of FRB 121102. The modulation index due to refractive scintillation is $\sim (\nu/\nu_t)^{17/30} = 0.15$ at $\nu = 1.4$ GHz; this is also negligible, in particular given the uncertainty in specifying the characteristic flux density of FRB 121102 discussed above. At Parkes, the HTRU and SUPERB surveys cover the sky outside the Galactic plane (Galactic latitudes $|b| > 15$ deg for the HTRU survey Keith et al. 2010; Champion et al. 2016) in an unbiased sense. Approximately 20% of the sky has $\nu_t \lesssim 1.4$ GHz (Walker 1998; Cordes & Lazio 2002), and the Parkes surveys are therefore generally in the strong scattering regime. Nonetheless, the wide fractional bandwidth of the Parkes receiving system ($\sim 25\%$), combined with the dramatic dependence of the diffractive scintillation bandwidth on frequency, implies that special conditions are required for only a single scintle of an extragalactic source to be present within the Parkes band. Refractive scintillation is likely the dominant effect on Parkes FRB detections, with typical modulation indices of ~ 0.5 . As the probability density function of refractive-scintillation intensity variations is only mildly skewed (Rickett et al. 1984), the expectation for the number

of objects like FRB 121102 present in the Parkes surveys is not likely to be very sensitive to the effects of scintillation. In fact, co-opting the argument of Macquart & Johnston (2015), scintillation may cause a boost in the number of objects like FRB 121102 detected at higher Galactic latitudes by Parkes, relative to my analysis.

Therefore, the best interpretation of Fig. 8 that can be presented here is that the HTRU and SUPERB surveys at Parkes could expect to contain up to three analogues of FRB 121102, if these analogues, presumably less distant than FRB 121102, lie above the Parkes detection threshold. The local-Universe location of these analogues suggests that the $\log N$ - $\log F$ of this population is unlikely to be flatter than $F^{-3/2}$, as I have assumed in producing Fig. 8. The best candidate analogues of FRB 121102 among the Parkes sample are clearly FRBs 121002, 130729, and possibly 140514. Like the pulses from FRB 121102, these Parkes FRBs show complex temporal structure, and in the cases of FRBs 130729 and 140514, spectral structures concentrated in ≈ 100 MHz bands.

5 CONCLUDING DISCUSSION

I return first to the question of how an FRB may be defined. All FRBs are fundamentally bursts of radio waves which exhibit levels of dispersion that exceed predictions for the Milky-Way ionised ISM column density along their specific sightlines. Beyond this, FRBs exhibit a broad diversity of (dedispersed) durations, scattering signatures, flux densities, and intrinsic temporal and spectral structures. In this paper, I have presented an analysis of the individual properties of the sample of seventeen FRBs detected at the Parkes telescope with the thirteen-beam L-band receiver. Eight of these FRBs show signatures of scattering at levels significantly greater than expected from the Milky Way, with scattering timescales at 1 GHz ranging between 0.005 – 32 ms. After accounting for the scattering, only five Parkes FRBs have pulse widths that are greater than expected from intra-channel smearing caused by their dispersions. The fluences of the Parkes FRB sample span a range greater than 0.7 – 400 Jy ms.

My analysis highlights the utility of searching for FRBs with systems that may better resolve the intrinsic pulse durations, because a substantial fraction of FRBs (6/17 at Parkes) are temporally unresolved. Such systems would require finer filterbank channel widths and better time resolutions than currently available, which could be achieved using coherent dedispersion techniques or observations at frequencies above the L-band. Better temporal resolution will also provide a boost in S/N for short-duration FRBs. Higher-frequency observations have the added bonus of being less affected by the temporal broadening observed in 7/17 Parkes FRBs; the characteristic spectra of FRBs are poorly constrained, and the repeating FRB 121102 has been observed at frequencies up to 5 GHz. Avoiding the effects of scattering may again provide a boost in S/N because of

shorter pulse durations, and may indeed provide sensitivity to a population of FRBs that are too broad to be detected in the L-band. Conversely, the effects of scattering must be taken into account in predicting FRB detection rates for lower-frequency experiments such as the Canadian Hydrogen Intensity Mapping Experiment (CHIME; e.g., Ng et al. 2017) and the Hydrogen Intensity and Real-time Analysis Experiment (HIRAX; Newburgh et al. 2016).

On the other hand, a search for long-duration FRBs at all frequencies may also be fruitful. Although the number of false candidates in single-dish observations increases rapidly with increasing pulse duration (Burke-Spolaor & Bailes 2010), and the detection S/N decreases as the square-root of the duration for constant fluence, such a search could be carried out by a sensitive interferometric system such as those being commissioned for the Jansky Very Large Array.⁴ There appears to be no reason to expect all FRBs to have the “millisecond” duration often quoted in the literature, beyond the effects of intra-channel dispersion smearing and scattering, and the increased sensitivity to narrower pulses.

My revised estimates of FRB scattering timescales, $\tau_{1\text{ GHz}}$, reveal moderate evidence for a relation between $\tau_{1\text{ GHz}}$ and the extragalactic DM (DM_E), similar to that observed for pulsars in the Milky Way (Fig. 4). The one outlier is FRB 010724, which has $\tau_{1\text{ GHz}} = 25 \pm 5$ ms for a low $DM_E = 288$ pc cm⁻³. The existence of such a relation, if supported by further observations, suggests that FRBs are predominantly dispersed in a medium within which they are also scattered, and for which the scattering strength increases for larger DM. This medium could be the ISM of FRB host galaxies, which would imply modest FRB distances, or the IGM or intervening collapsed systems. Observations of scattering in FRBs with distance measurements, obtained for example through localisation and the identification of host galaxies, could resolve the nature of the scattering and dispersing medium.

Although it appears that Parkes FRBs detected in individual beams of the multibeam receiver can have their fluences constrained to within a factor of five with 95% confidence, this is insufficient to directly estimate the FRB flux-density distribution (logN-logF). My analysis is therefore unable to distinguish between the case of a uniform distribution of FRB sources in the nearby Universe, and the flatter logN-logF distribution expected for a cosmological or evolving FRB population.

Finally, although the repeating FRB 121102 is an outlier among the FRB population in its repeat rate and the low fluences of most of its bursts, it is not demonstrably unique in its class of progenitor. The rate of repeats within the Parkes FRB population is lower than that of FRB 121102, and most Parkes FRBs have simpler temporal and spectral structures. However, some Parkes FRBs are similar in their morphologies to bursts from FRB 121102, and statistical arguments suggest that it is possible that up to three

objects like FRB 121102 have already been detected in surveys at Parkes. In a broader context, it is quite possible for all FRBs to be emitted by the same class of astrophysical object, but for such objects at different evolutionary stages to emit FRBs with different luminosity functions and rates.

ACKNOWLEDGEMENTS

I thank R. Shannon, H. Vedantham and S. Kulkarni for useful discussions in the course of this work. I also acknowledge the efforts of the FRB Catalogue team in maintaining the publicly accessible FRB database. I thank the referee for useful comments that helped improve the manuscript.

APPENDIX A: A SIGNAL MODEL FOR FRBS

In this section, I summarise the signal model for the Parkes FRBs analysed in this paper, and point out specific assumptions that I make. The voltage signal, V , presented to the AFB and BPSR backends at time t can be represented as follows:

$$V(t) = N(t) + h_{\text{IM}} * F(t), \quad (\text{A1})$$

where $N(t)$ is the receiver noise contribution, $h_{\text{IM}}(t)$ is a filter that encapsulates the effects of the ISM and IGM on the signal and $F(t)$ is proportional to the measured time-varying electric field of the FRB in a single polarisation. I assume that the signal is unpolarised, although this is not particularly relevant to my work. I assume that samples of the receiver noise $N(t)$ can be described by a time-stationary normal distribution, with zero mean and variance σ_N^2 (i.e., $\mathcal{N}(0, \sigma_N^2)$). This assumption neglects the potential effects of RFI. The FRB signal can be expressed as $S(t) = A(t)M(t)$, where $A(t)$ is an amplitude envelope, and $M(t)$ is again Gaussian with distribution $\mathcal{N}(0, \sigma_M^2)$. I further assume that $\sigma_M \ll \sigma_N$; that is, I do not account for “self-noise” in estimates of FRB properties because FRBs typically contribute negligibly to the system temperature (although see Ravi et al. 2016). Finally, I note that $V(t)$ is band-limited, and thus correlated on short timescales.

To illustrate my assumptions for the ISM/IGM effects, consider the Fourier transform of $V(t)$:

$$\tilde{V}(\nu) = \tilde{N}(\nu) + \tilde{h}_{\text{IM}}\tilde{S}(\nu), \quad (\text{A2})$$

where a tilde indicates a frequency-domain quantity. I assume that the ionised-medium filter \tilde{h}_{IM} can be expressed as the product of the standard cold, sparse plasma dispersion kernel, \tilde{h}_{DM} (Hankins 1971), and the pulse broadening function (PBF) caused by multi-path propagation, \tilde{h}_{PBF} . That is,

$$\tilde{h}_{\text{IM}} = \tilde{h}_{\text{DM}}\tilde{h}_{\text{PBF}}. \quad (\text{A3})$$

The assumption that \tilde{h}_{DM} and \tilde{h}_{PBF} are separable is valid for most, although perhaps not all, pulsars in the Galaxy (Cordes et al. 2016). I assume a one-sided exponential form

⁴ <https://caseyjlaw.github.io/realfast/>

for the PBF in the time domain, corresponding to the thin-screen scattering model (Cronyn 1970), wherein

$$h_{\text{PBF}}(t) = e^{-t/\tau} H(t)n(t), \quad (\text{A4})$$

where τ is the scattering timescale, $H(t)$ is the Heaviside step function, and $n(t)$ is a standard-normal random process.

The AFB and BPSR hardware are used to estimate the signal power at specific frequencies, ν_0 , within bandwidths $\Delta\nu$ and times Δt . I model this as follows:

$$\hat{S}(\nu_0, t) = \int_{t-\Delta t/2}^{t+\Delta t/2} |g(t') * V(t')|^2 dt', \quad (\text{A5})$$

where $g(t')$ is the time-domain representation of the filter corresponding to a single filterbank channel. I assume the following form for the frequency-domain filter:

$$\tilde{g}(\nu) = \sqrt{\frac{2}{\pi\Delta\nu^2}} e^{-2(\nu-\nu_0)^2/\Delta\nu^2}. \quad (\text{A6})$$

That is, I assume that the response of each filterbank channel is a Gaussian function with a standard deviation of $\Delta\nu/2$. Although this model does not accurately represent the responses of the analogue filters of the AFB or the polyphase-filterbank channels of BPSR, it appears adequate given the quality of the FRB data. The characteristic impulse-response timescale of the estimates of $\hat{S}(\nu_0, t)$ is therefore $1/\Delta\nu$; for both the AFB and BPSR, $\Delta t \gg 1/\Delta\nu$.

REFERENCES

- Bannister K. W., Madsen G. J., 2014, *MNRAS*, 440, 353
 Burke-Spolaor S., Bailes M., 2010, *MNRAS*, 402, 855
 Burke-Spolaor S., Bannister K. W., 2014, *ApJ*, 792, 19
 Caleb M., Flynn C., Bailes M., Barr E. D., Hunstead R. W., Keane E. F., Ravi V., van Straten W., 2016, *MNRAS*, 458, 708
 Champion D. J., Petroff E., Kramer M., Keith M. J., Bailes M., Barr E. D., Bates S. D., Bhat N. D. R., Burgay M. e. a., 2016, *MNRAS*, 460, L30
 Chatterjee S., Law C. J., Wharton R. S., Burke-Spolaor S., Hessels J. W. T., Bower G. C., et al. 2017, *Nat*, 541, 58
 Connor L., Pen U.-L., Oppermann N., 2016, *MNRAS*, 458, L89
 Cordes J. M., Lazio T. J. W., 2002, *ArXiv Astrophysics e-prints*
 Cordes J. M., McLaughlin M. A., 2003, *ApJ*, 596, 1142
 Cordes J. M., Shannon R. M., Stinebring D. R., 2016, *ApJ*, 817, 16
 Cordes J. M., Weisberg J. M., Frail D. A., Spangler S. R., Ryan M., 1991, *Nat*, 354, 121
 Cordes J. M., Wharton R. S., Spitler L. G., Chatterjee S., Wasserman I., 2016, *ArXiv e-prints*
 Cronyn W. M., 1970, *Science*, 168, 1453
 Dolag K., Gaensler B. M., Beck A. M., Beck M. C., 2015, *MNRAS*, 451, 4277
 Foreman-Mackey D., Hogg D. W., Lang D., Goodman J., 2013, *PASP*, 125, 306
 Gehrels N., 1986, *ApJ*, 303, 336
 Gupta A., Mathur S., Krongold Y., Nicastro F., Galeazzi M., 2012, *ApJ*, 756, L8
 Hankins T. H., 1971, *ApJ*, 169, 487
 Hickish J., Abdurashidova Z., Ali Z., Buch K. D., Chaudhari S. C., Chen H. e. a., 2016, *Journal of Astronomical Instrumentation*, 5, 1641001
 Hotan A. W., van Straten W., Manchester R. N., 2004, *Proc. Astron. Soc. Aust.*, 21, 302
 Katz J. I., 2016, *ApJ*, 818, 19
 Keane E. F., Barr E. D., Jameson A., Morello V., Caleb M., Bhandari S., Petroff E. e. a., 2017, *ArXiv e-prints*
 Keane E. F., Johnston S., Bhandari S., Barr E., Bhat N. D. R., Burgay M., Caleb M. e. a., 2016, *Nat*, 530, 453
 Keane E. F., Petroff E., 2015, *MNRAS*, 447, 2852
 Keane E. F., Stappers B. W., Kramer M., Lyne A. G., 2012, *MNRAS*, 425, L71
 Keith M. J., Jameson A., van Straten W., Bailes M., Johnston S., Kramer M., Possenti A., Bates S. D., Bhat N. D. R., Burgay M., Burke-Spolaor S., D'Amico N., Levin L., McMahon P. L., Milia S., Stappers B. W., 2010, *MNRAS*, 409, 619
 Li L., Huang Y., Zhang Z., Li D., Li B., 2016, *ArXiv e-prints*
 Lorimer D. R., Bailes M., McLaughlin M. A., Narkevic D. J., Crawford F., 2007, *Sci*, 318, 777
 Lorimer D. R., Karastergiou A., McLaughlin M. A., Johnston S., 2013, *MNRAS*, 436, L5
 Luan J., Goldreich P., 2014, *ApJ*, 785, L26
 Macquart J.-P., Johnston S., 2015, *MNRAS*, 451, 3278
 Macquart J.-P., Koay J. Y., 2013, *ApJ*, 776, 125
 Manchester R. N., Hobbs G. B., Teoh A., Hobbs M., 2005, *AJ*, 129, 1993
 Manchester R. N., Lyne A. G., Camilo F., Bell J. F., Kaspi V. M., D'Amico N., McKay N. P. F., Crawford F., Stairs I. H., Possenti A., Kramer M., Sheppard D. C., 2001, *MNRAS*, 328, 17
 Marcote B., Paragi Z., Hessels J. W. T., Keimpema A., van Langevelde H. J., Huang Y., et al. 2017, *ApJ*, 834, L8
 Masui K., Lin H.-H., Sievers J., Anderson C. J., Chang T.-C., Chen X., Ganguly A., Jarvis M., Kuo C.-Y., Li Y.-C., Liao Y.-W., McLaughlin M., Pen U.-L., Peterson J. B., Roman A., Timbie P. T., Voytek T., Yadav J. K., 2015, *Nat*, 528, 523
 Newburgh L. B., Bandura K., Bucher M. A., Chang T.-C., Chiang H. C., Cliche J. F., et al. 2016, in *Society of Photo-Optical Instrumentation Engineers (SPIE) Conference Series Vol. 9906 of Proc. SPIE, HIRAX: a probe of dark energy and radio transients.* p. 99065X
 Ng C., Vanderlinde K., Paradise A., Klages P., Masui K., Smith K., Bandura K., Boyle P. J., Dobbs M., Kaspi V., Renard A., Shaw J. R., Stairs I., Tret'yakov I., 2017, *ArXiv e-prints*
 Oppermann N., Connor L. D., Pen U.-L., 2016, *MNRAS*,

- 461, 984
- Petroff E., Bailes M., Barr E. D., Barsdell B. R., Bhat N. D. R., Bian F., Burke-Spolaor S., Caleb M., Champion D. e. a., 2015, *MNRAS*, 447, 246
- Petroff E., Barr E. D., Jameson A., Keane E. F., Bailes M., Kramer M., Morello V., Tabbara D., van Straten W., 2016, *ArXiv e-prints*
- Petroff E., Burke-Spolaor S., Keane E. F., McLaughlin M. A., Miller R., Andreoni I., Bailes M., Barr E. D., Bernard S. R., Bhandari S., et al. 2017, *MNRAS*, 469, 4465
- Petroff E., Johnston S., Keane E. F., van Straten W., Bailes M., Barr E. D., Barsdell B. R., Burke-Spolaor S., Caleb M., Champion D. J., Flynn C., Jameson A., Kramer M., Ng C., Possenti A., Stappers B. W., 2015, *MNRAS*, 454, 457
- Petroff E., van Straten W., Johnston S., Bailes M., Barr E. D., Bates S. D., et al. 2014, *ApJ*, 789, L26
- Ravi V., Shannon R. M., Bailes M., Bannister K., Bhandari S., Bhat N. D. R., Burke-Spolaor S., Caleb M., Flynn C., Jameson A., Johnston S., Keane E. F., Kerr M., Tiburzi C., Tuntsov A. V., Vedantham H. K., 2016, *Science*, 354, 1249
- Ravi V., Shannon R. M., Jameson A., 2015, *ApJ*, 799, L5
- Rickett B. J., Coles W. A., Bourgois G., 1984, *A&A*, 134, 390
- Scholz P., Spitler L. G., Hessels J. W. T., Chatterjee S., Cordes J. M., Kaspi V. M., et al. 2016, *ApJ*, 833, 177
- Spitler L. G., Scholz P., Hessels J. W. T., Bogdanov S., Brazier A., Camilo F., Chatterjee S., Cordes J. M., Crawford F. e. a., 2016, *Nat*, 531, 202
- Staveley-Smith L., Wilson W. E., Bird T. S., Disney M. J., Ekers R. D., Freeman K. C., Haynes R. F., Sinclair M. W., Vaile R. A., Webster R. L., Wright A. E., 1996, *Proc. Astron. Soc. Aust.*, 13, 243
- Tendulkar S. P., Bassa C. G., Cordes J. M., Bower G. C., Law C. J., Chatterjee S., et al. 2017, *ApJ*, 834, L7
- Thornton D., Stappers B., Bailes M., Barsdell B., Bates S., Bhat N. D. R., Burgay M., Burke-Spolaor S., Champion D. J., Coster P. e. a., 2013, *Sci*, 341, 53
- van Straten W., Bailes M., 2011, *Proc. Astron. Soc. Aust.*, 28, 1
- Vedantham H. K., Ravi V., Hallinan G., Shannon R., 2016, *ArXiv e-prints*
- Walker M. A., 1998, *MNRAS*, 294, 307
- Williamson I. P., 1972, *MNRAS*, 157, 55
- Yan W. M., Manchester R. N., van Straten W., Reynolds J. E., Hobbs G., Wang N., Bailes M., Bhat N. D. R., Burke-Spolaor S., Champion D. J., Coles W. A., Hotan A. W., Khoo J., Osłowski S., Sarkissian J. M., Verbiest J. P. W., Yardley D. R. B., 2011, *MNRAS*, 414, 2087